ACS Energy LETTERS

Cite This: ACS Energy Lett. 2018, 3, 78−84

LETTER

Bimetallic Carbide as a Stable Hydrogen Evolution Catalyst in Harsh Acidic Water

Meng Yang Zu,[†] Peng Fei Liu,[†] Chongwu Wang,[†] Yun Wang,[‡] Li Rong Zheng,[#] Bo Zhang,[§] Huijun Zhao,[‡] and Hua Gui Yang*[,†]

[†]Key Laboratory for Ultrafine Materials of Ministry of Education, School of Materials Science and Engineering, East China University of Science and Technology, Shanghai 200237, China

[‡]Centre for Clean Environment and Energy, Gold Coast Campus, Griffith University, Southport, Queensland 4222, Australia

[§]State Key Laboratory of Molecular Engineering of Polymers, Department of Macromolecular Science, Fudan University, Shanghai 200438, China

[#]Institute of High Energy Physics, Chinese Academy of Sciences, Beijing 100049, China

Supporting Information

ABSTRACT: Cheap, efficient, and stable hydrogen evolution reaction (HER) electrocatalysts have long been pursued, owing to their scientific and technological importance. Currently, platinum has been regarded as the benchmarked HER electrocatalyst. Unfortunately, the low abundance and high cost impede its industrial applications. Here, we synthesize bimetallic carbide Mo_6Ni_6C grown on nickel foam as a HER catalyst, delivering a low overpotential of −51 mV at −10 mA cm^{-2} in 0.5 M H_2SO_4 for more than 200 h, which is among the best reported benchmarked HER catalysts in acid to date. On the basis of experimental observations and theoretical modeling, we ascribe the good activity to the proper Gibbs free energy of adsorbed hydrogen ($\Delta G(H^*)$) for the carbon active sites and attribute the stability to the corrosion-stable Mo−Mo bonds in the crystal structure. This work demonstrates the possibility for Mo_6Ni_6C to be one of the best candidates for HER electrocatalysts in the large-scale electrolysis industry.

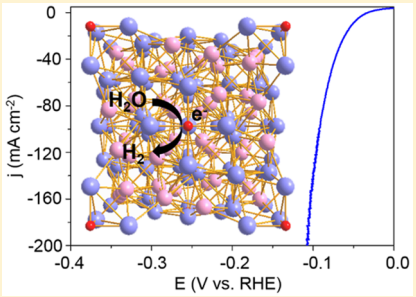

Hydrogen production via electrolysis is a vital process in several developing clean-energy technologies.[1−3] However, currently, the efficiency of the hydrogen evolution reaction (HER) is too low to be economically competitive, considering that 4.5−5.0 kWh/m^3 of H_2 energy on average is needed for conventional industrial electrolyzers, which restricts its applications among all of the hydrogen production industries (just 4% of about 500 billion Nm^3/year) in total around the world.[4] Therefore, to further increase the efficiency and lower the cost of this process, active and stable hydrogen evolution electrocatalysts are urgently needed, especially for the industrial operation in harsh acidic and alkaline media. Although platinum (Pt) has been regarded as the optimum HER electrocatalyst, the low abundance and corresponding high cost further restrict its large-scale utilization.[5−7] Hence, it still remains a great challenge to develop a low-cost and high-activity HER electrocatalyst in harsh electrolytes for long-time durable hydrogen production.

Very recently, Zhang et al.,[8] Chen et al.,[9] and Csernica et al.[10] prepared $MoNi_4/MoO_2$, $MoNi_4/MoO_{3-x}$, and Mo_7Ni_7 as highly active catalysts with sustained H_2 production in 1.0 M KOH, and they are demonstrated as record alkaline HER electrocatalysts to date. However, these NiMo alloys can easily get deactivated under the working conditions because of rapid corrosion and gradual oxidation, especially in acidic media, in which they could not even survive for a pretty short time.[5,11] In response, we aim to improve the performance of these alloy-based HER catalysts in acid by employing a subtle modification strategy. Previous work suggests that bimetallic compounds, such as bimetallic sulfides,[12−14] carbides,[15−17] nitrides,[18,19] and phosphides,[20,21] usually possess better durability than alloys, among which carbides and nitrides have emerged as the best candidates because the interstitial carbon and nitrogen atoms could modify the nature of the d orbital in the parent metal, thus increasing the s−p electrons count and giving rise to the catalytic properties similar to the noble metal Pt.[22−26] For example, Green et al.[27] found that in the field of pyridine hydrodenitrogenation catalysis, CoMo-based compounds show activity decreasing in the order of $CoMoC_x \approx CoMoN_x \approx CoMoO_x > CoMoS_x$, and the stability order of the first three catalysts is $CoMoC_x > CoMoN_x > CoMoO_x$. Considering the mechanism similarities between the HER and HDN (both adsorption and desorption processes of the proton), we anticipate that bimetallic carbide is quite possible to possess

Received: October 11, 2017
Accepted: November 28, 2017
Published: November 28, 2017

DOI: 10.1021/acsenergylett.7b00990
ACS Energy Lett. 2018, 3, 78−84

better stability compared to NiMo alloys, especially in acidic water.

Herein, for the first time, we rationally designed a bimetallic carbide Mo_6Ni_6C uniformly grown on Ni foam (Mo_6Ni_6C/NF) as an active and ultrastable electrocatalyst for sustainable HER in harsh acidic media. The density functional theory (DFT) calculations elucidate that the Mo_6Ni_6C catalyst is intrinsically metallic and possesses a moderate Gibbs free energy of adsorbed hydrogen ($\Delta G(H^*)$) around 0 eV like Pt, which renders Mo_6Ni_6C highly active toward the HER process. X-ray absorption fine structure (XAFS) analysis of Mo_6Ni_6C confirms the existence of acid-stable Mo−Mo bonds,[28,29] which potentially stabilize its architecture, leading to better stability. Consequently, Mo_6Ni_6C/NF exhibits excellent HER performance for achieving a low overpotential (η) of −51 mV at a current density (j) of −10 mA cm^{-2} for at least 200 h in 0.5 M H_2SO_4, surpassing other available HER catalysts to date. Simultaneously, it maintains equivalently distinguished performance in 1.0 M KOH for delivering a j of −10 mA cm^{-2} for at least 300 h at an η of −34 mV. These findings suggest that bimetallic carbides could serve as a promising group of HER electrocatalysts in a harsh acidic environment, and its extraordinarily high activity and stability open up avenues to replace platinum in technologies relevant to renewable energies, such as the large-scale application of alkaline water electrolysis (AWE) and a proton exchange membrane (PEM) electrolyzer.

The schematic representations of Mo_6Ni_6C, NiMo, and Mo_2C are shown in Figures 1, S1, and S2. It is mentionable that

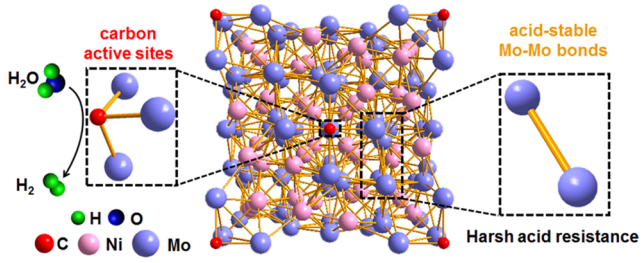

Figure 1. Schematic representation of the structure of Mo_6Ni_6C, demonstrating the origin of its excellent HER activity from carbon active sites and outstanding stability form corrosion-stable Mo−Mo bonds.

Mo−Mo bonds exist in Mo_6Ni_6C, resembling acid-stable Mo_2C,[30] while no Mo−Mo bonds exist in NiMo alloy. To characterize the crystal structure of Mo_6Ni_6C, powder X-ray diffraction (XRD) was conducted. As shown in Figures 2a and S3, the synthesized sample was well matched with the reference XRD pattern of cubic Mo_6Ni_6C (JCPDS No. 65-4436). Notably, the apparent diffraction peak centered at 40.5° is ascribed to the (422) plane of Mo_6Ni_6C. XRD patterns of the samples synthesized via different temperatures and Ni:Mo ratios are also shown in Figure S4.

Figure S5a,b shows the photographs of Mo_6Ni_6C/NF before and after being stretched, indicating that the material can be flexed well without undergoing structural damage. When the Ni foam substrate was enlarged to 3 cm × 4 cm (Figure S5c), the surface of the Ni foam was still well-proportioned as previous samples. Scanning electron microscope (SEM) images and corresponding elemental mappings reveal that the synthesized materials uniformly cover the surfaces of Ni foam (Figures 2b, S6, and S7). Furthermore, high-resolution SEM images clearly show that Mo_6Ni_6C/NF consists of some clusters of rods with a mean diameter of around 1 μm, which are built up by a set of nanoparticles of 50 nm in average (Figures 2c, S8, and S9). Similarly, the covered Mo_6Ni_6C materials are also made up by the nanoparticles of the same size (Figure 2d). The transmission electron microscope (TEM) images of Mo_6Ni_6C are shown in Figures 2e and S10, which are consistent with the SEM image of rods and clusters composed of nanoparticles with an average size of 50 nm. TEM and high-resolution TEM (HRTEM) images (Figure 2f,g) further confirm that a series of lattice fringes give interplanar distances of 0.222 nm, corresponding to the (422) crystallographic planes of the Mo_6Ni_6C phase, which agrees well with XRD results. The corresponding selected area electron diffraction (SAED) pattern of Mo_6Ni_6C confirms that it owns high crystallinity (inset of Figure 2g). Furthermore, to optimize the performance of Mo_6Ni_6C, we adjusted the synthesis temperatures and initial ratios of precursors, and the corresponding SEM images are listed in Figures S11 and S12. We found that the temperature influences the particle size of Mo_6Ni_6C and the Ni:Mo ratio affects the density of clusters of rods.

The X-ray photoelectron spectroscopy (XPS) spectra of Mo 3d and Ni $2p_{3/2}$ for Mo_6Ni_6C/NF are shown in Figure 3a,b. Mo 3d spectra are split into $3d_{5/2}$ and $3d_{3/2}$ peaks because of the spin−orbital coupling feature, and the peaks located at binding energies of 227.8 and 231.1 eV are assigned to metallic Mo ($3d_{5/2}$ and $3d_{3/2}$, respectively); the other peaks are attributed to surface oxidized phases.[31,32] Similarly, it can be observed that the strong peak at 852.4 eV with its satellite at 857.2 eV belongs to metallic Ni, and the other peaks are assigned to Ni^{x+}.[33,34] The low valence states of Mo and Ni certify the metallic nature of Mo_6Ni_6C, which is beneficial to produce high catalytic activities of the HER process.[35,36] Further comparison analyses have also been taken among the samples with different synthesis temperatures (Figure S13). It is worth mentioning that the C 1s and Ni 2p spectra of all of the samples are similar,[33,34,37,38] but the characteristic peaks for the Mo 3d spectrum of the sample synthesized at 500 °C (Mo_6Ni_6C/NF/500) are quite different from others, and the biggest difference is that Mo^0 signals at around 227.8 and 231.1 eV are missing. Further, we conducted galvanostatic measurement for Mo_6Ni_6C/NF/500 in 0.5 M H_2SO_4, discovering its poor stability compared to Mo_6Ni_6C/NF (Figure S14). Considering that the materials also uniformly cover the surfaces of Ni foam for Mo_6Ni_6C/NF/500 (Figure S11), we conclude that Mo−Mo bonds get a contribution in the catalysts' durability, which is consistent with XAFS analysis and previous studies.[27]

To further probe the bulk fine structures of the catalysts, XAFS characterizations were carried out. In Figure 3c, only the NiMo alloy sample exhibits an obvious oxidation peak at around 20005.2 eV, which is probably caused by the easy oxidation in air. However, for the Ni K-edge XANES spectra, the Mo_6Ni_6C exhibits a similar valence like NiMo alloy, confirming the metallic feature of the catalyst (Figure 3d). As shown in Figure 3e, the Fourier transforms (FTs) of the XAFS spectra collected at the Mo K-edge region reveal that considerable Mo−Mo bonds exist in Mo_6Ni_6C and Mo_2C. For comparison, no apparent signals centered at around 2.4 and 2.7 Å were detected in NiMo alloy. In addition, the peak at around 1.5 Å is associated with Mo−C bonds,[35] consistent with Mo−C bonding in the crystal structure of Mo_6Ni_6C. The FTs of the XAFS spectra for Ni K-edge demonstrated the existence of Ni−Ni bonds in the Mo_6Ni_6C sample, further illustrating its

DOI: 10.1021/acsenergylett.7b00990
ACS Energy Lett. 2018, 3, 78−84

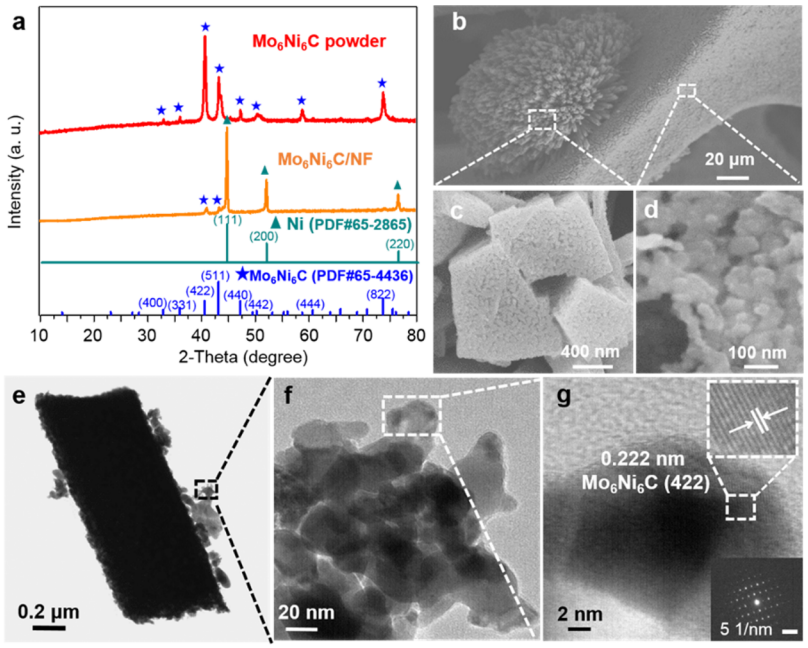

Figure 2. (a) XRD patterns of Mo_6Ni_6C powder and Mo_6Ni_6C/NF. (b–d) SEM images of Mo_6Ni_6C/NF at different magnifications. (e–g) TEM images of Mo_6Ni_6C. Inset of (g): HRTEM image and corresponding SAED pattern of Mo_6Ni_6C.

metallic property (Figure 3f). The corresponding FTs of k^3-weighted EXAFS oscillations are shown in Figure S15. Overall, XAFS unambiguously proved the metallic feature of the Mo_6Ni_6C, with Mo–Mo and Ni–Ni bonds in the structure.

To evaluate the HER performances of Mo_6Ni_6C/NF, we investigate the linear sweep voltammetry (LSV) curves of all of the samples in a typical three-electrode system with 0.5 M H_2SO_4 and 1.0 M KOH as the electrolyte. First, in the harsh acidic environment, Mo_6Ni_6C/NF possesses high activity (Figure 4a) for showing excellent HER catalytic activity with j values of −10, −20, and −100 mA cm^{-2} at η values of −51, −61, and −93 mV (−10 mA cm^{-2} at −44 mV for Pt/C/NF, −217 mV for NiMo/NF, −288 mV for Mo_2C/NF, and −382 mV for blank NF), standing at the forefront of the HER field. Moreover, to weaken the influence of the electrical contact between the particles and Ni foam, we reloaded the Mo_6Ni_6C powder, which was scraped off from the Ni foam substrate, onto a Ni foam substrate (denoted as Mo_6Ni_6C powder/NF) to test the LSV (Figure S16). It could be observed that Mo_6Ni_6C powder/NF still performs better than Mo_2C and $MoNi_4$ loaded on Ni foam in a similar dip-coating method with the same loading. Additionally, the LSV plots of the samples synthesized at different temperatures and Ni:Mo ratios are shown in Figures S17 and S18. Correspondingly, the Nyquist spectra reveal that Mo_6Ni_6C/NF has a fast charge transport process (Figure 4b), and the equivalent circuit used for fitting the Nyquist plots is shown in the inset of Figure 4b. The Tafel slope of Mo_6Ni_6C/NF is 35.70 mV dec^{-1}, which is much lower than the other control samples except for Pt/C/NF (Figure 4c). The effective active surface area (ECSA) of Mo_6Ni_6C/NF was estimated from the double layer capacitance (C_{dl}) as C_{dl} is linearly proportional to the ECSA. The C_{dl} of Mo_6Ni_6C/NF is about 0.77 F cm^{-2} in 0.5 M H_2SO_4 (Figures 4d and S19), larger than that of NiMo/NF, Pt/C/NF, and Mo_2C/NF, guaranteeing a large ECSA, which also synergistically contributes to the excellent HER activity. However, when normalized by ECSA, we found that the j of Mo_6Ni_6C/NF was still larger than that of compared samples (NiMo/NF and Mo_2C/NF), further revealing that Mo_6Ni_6C was intrinsically more active (Figure S20). Noteworthy, to evaluate the stability of Mo_6Ni_6C/NF, galvanostatic measurements were conducted in 0.5 M H_2SO_4 (Figure 5). A continuous HER process occurred to generate molecular hydrogen at a j value of −10 mA cm^{-2}. The Mo_6Ni_6C/NF electrode could maintain a j of −10 mA cm^{-2} at around −77 mV without apparent deactivation in acidic media for at least 200 h and a j of −40 mA cm^{-2} at around −100 mV for 20 h (Figure S21). To avoid the background current interfering with the evaluation of HER performance, a multistep current test was conducted (Figure S22). The current density started at −10 to −100 mA cm^{-2} with an increment of −10 mA cm^{-2} every 600 s. In the low current density range (below −100 mA cm^{-2}), the j and corresponding η values matched well with those tested in the polarization curves, suggesting that a low capacitance current existed in the HER potential range. In addition, the Faradaic efficiency (FE) for hydrogen evolution of this catalyst was evaluated, which was determined to be nearly 100% during the 10 h of electrolysis (inset of Figure 5). The corresponding video for the HER process under different overpotentials in acidic water is shown in Movie S1 (Supporting Information). For comparison, Movie S2 (Supporting Information) indicates that Mo_6Ni_6C/NF maintains a more rapid HER rate than Pt/C/NF under the same overpotentials, which obviously illustrates the better HER activity of Mo_6Ni_6C than Pt/C. To the best of our knowledge, such activity combined with ultrastable durability for the materials in acidic conditions, which are directly grown on Ni foams without any protective layers (graphene or amorphous carbon), has never been reported before.

As stated by Markovic et al.,[6] the HER activities of most catalysts in alkaline water are customarily around 2 or 3 orders of magnitude lower than those in acidic solutions because they are generally inefficient in the prior step of water dissociation. Fortunately, Mo_6Ni_6C/NF could overcome this obstacle and even possess better activity in the alkaline environment.

DOI: 10.1021/acsenergylett.7b00990
ACS Energy Lett. 2018, 3, 78–84

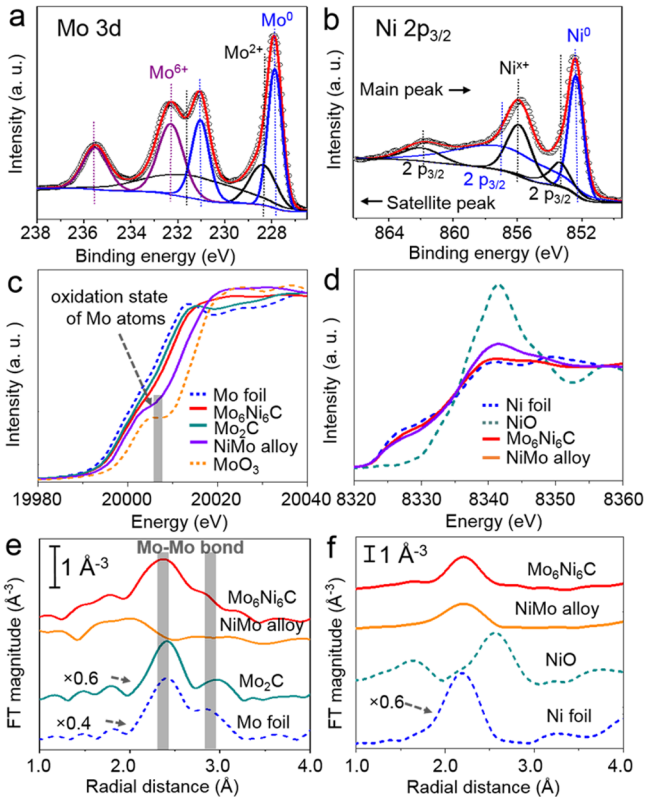

Figure 3. XPS spectra of Mo_6Ni_6C/NF for (a) Mo 3d and (b) Ni $2p_{3/2}$. (c) Mo K-edge XANES spectra for the samples of Mo_6Ni_6C, Mo foil, NiMo alloy, Mo_2C, and MoO_3. The oxidation state of Mo atoms for the NiMo alloy indicates that they get oxidized easily in the air. (d) Ni K-edge XANES spectra for the samples of Mo_6Ni_6C, NiMo alloy, Ni foil, and NiO. (e) FT of Mo K-edge EXAFS for the samples of Mo_6Ni_6C and controlled samples, revealing the existence of a Mo−Mo bond in the Mo_6Ni_6C. (f) FT of Ni K-edge EXAFS for the samples of Mo_6Ni_6C, NiMo alloy, Ni foil, and NiO, illustrating the existence of Ni−Ni bonds in the Mo_6Ni_6C sample, further illustrating its metallic property.

Mo_6Ni_6C/NF shows j values of −10, −20, and −100 mA cm^{-2} at η values of −34, −48, and −112 mV (Figure S23a), respectively. Correspondingly, the Nyquist spectra reveal that Mo_6Ni_6C/NF also has the fastest charge transport process among all of the controlled catalysts (Figure S23b) in 1.0 M KOH and displays a Tafel slope of 36.34 mV dec^{-1} (as shown in Figure S23c). The C_{dl} of Mo_6Ni_6C/NF is 1.18 F in 1.0 M KOH (Figure S23d). Galvanostatic measurements taken in alkaline media (Figures S24 and S25) could last for more than 300 h at a j of −10 mA cm^{-2} and 20 h at a j of −40 mA cm^{-2}, and the FE for hydrogen evolution was also determined to be nearly 100% during 10 h of electrolysis (inset of Figure S24). Moreover, a multistep current test was also conducted (Figure S26). The j and corresponding η values also matched well with those tested in the polarization curves below −100 mA cm^{-2}, indicating that a low capacitance current existed in the HER potential range. The corresponding video for the HER process under different overpotentials in 1.0 M KOH is shown in Movie S3 (Supporting Information). In general, such activity and stability of Mo_6Ni_6C are located in the top positions of the recently reported HER electrocatalysts, as compared in the Table S1 (Supporting Information).

To further confirm the structure stability of the bimetallic Mo_6Ni_6C after a long-time HER process, a series of characterizations were carried out. After the stability test, the XRD patterns of Mo_6Ni_6C/NF are shown in Figure S27, from which we could know that the intensity of those peaks for the Mo_6Ni_6C phase became slightly weaker after 200 h of operation in 0.5 M H_2SO_4. Nonetheless, the crystal structure still remains as Mo_6Ni_6C. For the sample measured in 1.0 M KOH, the XRD pattern is almost the same as the pristine one. Furthermore, after exposure to air for more than 120 days, the XRD pattern of Mo_6Ni_6C/NF was also tested, and a negligible difference was observed, as shown in Figure S28. Unlike NiMo alloy and Mo_2C, which are easy to get the surface oxidation exposed to air,[11,39,40] Mo_6Ni_6C also displays extraordinary stability in the air.

The morphologies of the catalyst before and after chronopotentiometric tests in 0.5 M H_2SO_4 and in 1.0 M KOH were also characterized. After the stability test in 0.5 M H_2SO_4, the rods seemed like they were somewhat melting on the surface (Figure S29), which may be caused by the harsh environment of acidic electrolyte. However, we could clearly see that the material still was composed of nanoparticles in nature, which covered the Ni foam uniformly, protecting the substrate from being corroded by the strong acid. The morphologies of Mo_6Ni_6C/NF after a 300 h durability test in 1.0 M KOH became a little different from those of the pristine, identifying that there is lamellar substance formed on the surface (Figure S30). Overall, the XRD characterizations clearly demonstrate that this bimetallic carbide Mo_6Ni_6C could sustain a strong acidic and alkaline solution for a continuous HER process, which would not be influenced by the morphologies. As supporting evidence, the digital photos of Mo_6Ni_6C/NF and controlled samples immersed in 0.5 M H_2SO_4 before and after 30 days are also shown in Figure S31. For comparison, we could observe that only Mo_6Ni_6C/NF did not change significantly, but others seemed to dissolve into the acidic solution to different extents.

DFT calculations were carried out to further pinpoint the origin of the excellent performance of Mo_6Ni_6C. First, the calculated density of states (DOS) images for Mo_6Ni_6C (Figure S32) confirm the metallic feature of Mo_6Ni_6C. For comparison, the total density of states (TDOS) and partial density of states (PDOS) of other controlled samples were also calculated. It can be found that the peaks of occupied states of Mo_6Ni_6C are higher at the lower energy range ([−8.0 eV, −4.0 eV]) in terms of those of Ni_3C and Mo_2C (Figures S33 and S34). It indicates that that Mo_6Ni_6C owns better stability, which is in agreement with the experimental observation. To further evaluate the electrocatalytic performance of Mo_6Ni_6C, we systematically examined ΔG(H*) on the Mo_6Ni_6C (422) surface by virtue of extensive first-principles DFT calculations (Figure S35). Because all Ni, Mo, and C atoms are in the topmost layer of the (422) surface, the adsorption of H on these three different sites is considered. It is found that carbon atoms on Mo_6Ni_6C (422) (denoted as C@Mo_6Ni_6C) possess the most optimum ΔG(H*), indicating that they may be the active sites for HER. Compared to some other materials,[41,42] C@Mo_6Ni_6C also outperforms them because its value of ΔG(H*) is closer to 0 (approximately 0.05 eV). Calculations of the activity and stability were further verified by experimental investigations, as shown above.

To test the viability of Mo_6Ni_6C/NF for large-scale water electrolysis, we constructed high-surface-area Mo_6Ni_6C/NF as the cathode and incorporated it into an alkaline electrolyzer. The anode was made by a two-step hydrothermal method of

DOI: 10.1021/acsenergylett.7b00990
ACS Energy Lett. 2018, 3, 78−84

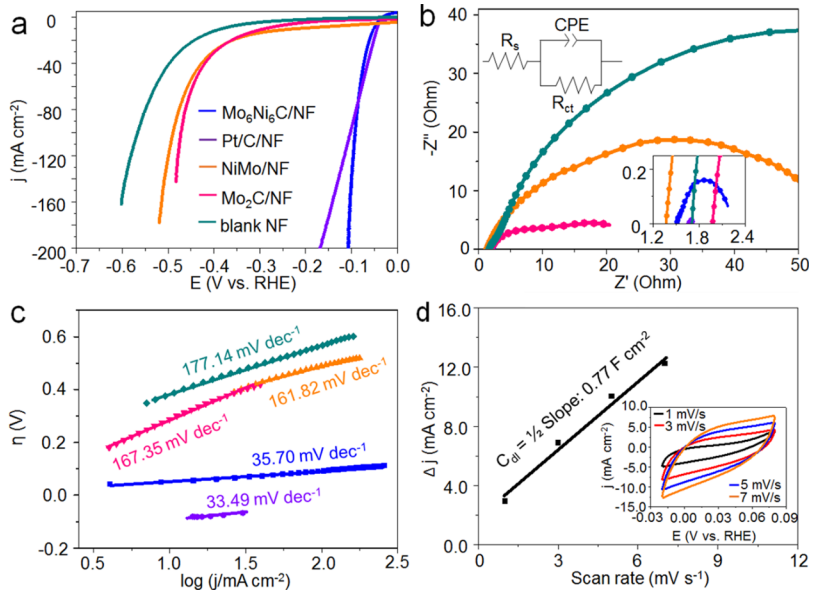

Figure 4. (a) LSV curves, (b) Nyquist, and (c) Tafel plots for HER for the samples of Mo_6Ni_6C/NF, Pt/C/NF, NiMo/NF, Mo_2C/NF, and blank Ni foam (the catalyst loading is about 18 mg cm^{-2} for every sample). Mo_6Ni_6C/NF possesses comparable series resistance and charge transport resistance among all of the controlled catalysts. The C_{dl} of Mo_6Ni_6C/NF in 0.5 M H_2SO_4 was assessed utilizing a series of cyclic voltammetry (CV) cycles at different scan rates. (d) Scan rate dependence of the current densities ($\Delta j = j_a - j_c$) for Mo_6Ni_6C/NF at 0.03 V vs RHE. Inset of (d): Cyclic voltammograms of Mo_6Ni_6C/NF at different scan rates (from 1 to 7 mV/s with an increment of 2 mV/s).

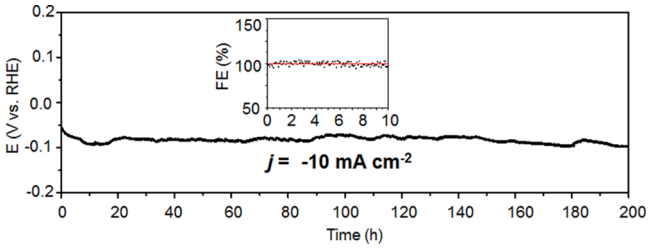

Figure 5. Chronopotentiometric curve of Mo_6Ni_6C/NF at j of −10 mA cm^{-2} for a continuous HER process. Inset: corresponding faradaic efficiency from gas chromatography measurement of evolved H_2 for 10 h of the chronopotentiometric test.

nickel iron diselenide on Ni foam ($Ni_xFe_{1-x}Se_2$/NF).[43] The anode was first tested separately in a three-electrode setup to assess its individual performance for the relevant reactions, which exhibited high activity in 1.0 M KOH electrolyte, requiring a 210 mV overpotential to drive oxygen production at 10 mA cm^{-2}, as shown in Figure S36. The electrodes were then loaded into a homemade single cell, and the resultant electrolyzer exhibited excellent performance, delivering 10 mA cm^{-2} at approximately 1.51 V consistently over a 25 h period at room temperature and at around 1.44 V at a temperature of 60 °C (Figure S37). The relevant details about the electrolyzer are shown in Figure S38. These results provide an initial assessment of the feasibility for using Mo_6Ni_6C/NF in operational water electrolysis systems.

In conclusion, for the first time, Mo_6Ni_6C has been discovered as a high-performance and low-cost electrocatalyst for hydrogen production. Impressively, it exhibits the lowest overpotential of −51 mV in acidic water at −10 mA cm^{-2}. More importantly, the catalyst shows no evidence of degradation following more than 200 h of operation in 0.5 M H_2SO_4. DFT calculations indicate that the most proper active sites for the Mo_6Ni_6C are carbon atoms on its (422) plane. Furthermore, the XAFS results confirm the presence of abundant Mo−Mo bonds in the structure, which leads to better stability for the catalyst. At the same time, Mo_6Ni_6C also shows outstanding performance in alkali for delivering a j value of −10 mA cm^{-2} at a η value of −34 mV for more than 300 h. The high intrinsic catalytic activity and chemical stability of Mo_6Ni_6C make it one of the most effective HER electrocatalysts, showing the potential to work in an operational device environment. These findings represent an important advancement toward expanding the scope of high-performance hydrogen evolution catalysts for large-scale applications of AWE and PEM electrolyzers.

■ ASSOCIATED CONTENT

Supporting Information

The Supporting Information is available free of charge on the ACS Publications website at DOI: 10.1021/acsenergylett.7b00990.

Experimental section, additional SEM and TEM figures, XRD, XPS, and XAFS analysis, electrochemical data, and Table S1 for comparison of HER performance (PDF)

Electrocatalytic hydrogen evolution at different overpotentials in 0.5 M H_2SO_4 (AVI)

Comparison of Pt/C and Mo_6Ni_6C at different overpotentials in 0.5 M H_2SO_4 (AVI)

Electrocatalytic hydrogen evolution at different overpotentials in 1.0 M KOH (AVI)

■ AUTHOR INFORMATION

Corresponding Author

*E-mail: hgyang@ecust.edu.cn.

ORCID

Peng Fei Liu: 0000-0003-0411-0488

Huijun Zhao: 0000-0003-3794-4497

Hua Gui Yang: 0000-0003-0436-8622

DOI: 10.1021/acsenergylett.7b00990
ACS Energy Lett. 2018, 3, 78−84

Notes

The authors declare no competing financial interest.

■ ACKNOWLEDGMENTS

This work was financially supported by the National Natural Science Foundation of China (21573068, 21503079), SRF for ROCS, SEM, SRFDP, the Program of Shanghai Subject Chief Scientist (15XD1501300), and the Shanghai Municipal Natural Science Foundation (14ZR1410200). The authors also thank the crew of the 1W1B beamline of the Beijing Synchrotron Radiation Facility for the constructive assistance in the XAFS measurements and data analyses.

■ REFERENCES

(1) Khaselev, O.; Turner, J. A. A Monolithic Photovoltaic-Photoelectrochemical Device for Hydrogen Production via Water Splitting. *Science* **1998**, *280*, 425−427.

(2) Carmo, M.; Fritz, D. L.; Mergel, J.; Stolten, D. A Comprehensive Review on PEM Water Electrolysis. *Int. J. Hydrogen Energy* **2013**, *38*, 4901−4934.

(3) Li, H.; Tsai, C.; Koh, A. L.; Cai, L.; Contryman, A. W.; Fragapane, A. H.; Zhao, J.; Han, H. S.; Manoharan, H. C.; Abild-Pedersen, F.; et al. Activating and Optimizing MoS_2 Basal Planes for Hydrogen Evolution through the Formation of Strained Sulphur Vacancies. *Nat. Mater.* **2015**, *15*, 48−53.

(4) Subbaraman, R.; Tripkovic, D.; Strmcnik, D.; Chang, K.-C.; Uchimura, M.; Paulikas, A. P.; Stamenkovic, V.; Markovic, N. M. Enhancing Hydrogen Evolution Activity in Water Splitting by Tailoring Li^+-$Ni(OH)_2$-Pt interfaces. *Science* **2011**, *334*, 1256−1260.

(5) Zou, X.; Zhang, Y. Noble Metal-Free Hydrogen Evolution Catalysts for Water Splitting. *Chem. Soc. Rev.* **2015**, *44*, 5148−5180.

(6) Nocera, D. G. The Artificial Leaf. *Acc. Chem. Res.* **2012**, *45*, 767−776.

(7) Staszak-Jirkovský, J.; Malliakas, C. D.; Lopes, P. P.; Danilovic, N.; Kota, S. S.; Chang, K.-C.; Genorio, B.; Strmcnik, D.; Stamenkovic, V. R.; Kanatzidis, M. G.; et al. Design of Active and Stable Co-Mo-S_x as pH-Universal Catalysts for the Hydrogen Evolution Reaction. *Nat. Mater.* **2015**, *15*, 197−203.

(8) Zhang, J.; Wang, T.; Liu, P.; Liao, Z.; Liu, S.; Zhuang, X.; Chen, M.; Zschech, E.; Feng, X. Efficient Hydrogen Production on $MoNi_4$ Electrocatalysts with Fast Water Dissociation Kinetics. *Nat. Commun.* **2017**, *8*, 15437.

(9) Chen, Y.-Y.; Zhang, Y.; Zhang, X.; Tang, T.; Luo, H.; Niu, S.; Dai, Z.-H.; Wan, L.-J.; Hu, J.-S. Self-Templated Fabrication of $MoNi_4$/MoO_{3-x} Nanorod Arrays with Dual Active Components for Highly Efficient Hydrogen Evolution. *Adv. Mater.* **2017**, *29*, 1703311.

(10) Csernica, P. M.; McKone, J. R.; Mulzer, C. R.; Dichtel, W. R.; Abruña, H. D.; DiSalvo, F. J. Electrochemical Hydrogen Evolution at Ordered Mo_7Ni_7. *ACS Catal.* **2017**, *7*, 3375−3383.

(11) Chen, W.-F.; Sasaki, K.; Ma, C.; Frenkel, A. I.; Marinkovic, N.; Muckerman, J. T.; Zhu, Y.; Adzic, R. R. Hydrogen-Evolution Catalysts Based on Non-Noble Metal Nickle-Molybdenum Nitride Nanosheets. *Angew. Chem., Int. Ed.* **2012**, *51*, 6131−6135.

(12) Li, J.-S.; Wang, Y.; Liu, C.-H.; Li, S.-L.; Wang, Y.-G.; Dong, L.-Z.; Dai, Z.-H.; Li, Y.-F.; Lan, Y.-Q. Coupled Molybdenum Carbide and Reduced Graphene Oxide Electrocatalysts for Efficient Hydrogen Evolution. *Nat. Commun.* **2016**, *7*, 11204.

(13) Zhu, J.; Sakaushi, K.; Clavel, G.; Shalom, M.; Antonietti, M.; Fellinger, T.-P. A General Salt-Templating Method to Fabricate Vertically Aligned Graphitic Carbon Nanosheets and Their Metal Carbide Hybrids for Superior Lithium Ion Batteries and Water Splitting. *J. Am. Chem. Soc.* **2015**, *137*, 5480−5485.

(14) Miao, J.; Xiao, F.-X.; Yang, H. B.; Khoo, S. Y.; Chen, J.; Fan, Z.; Hsu, Y.-Y.; Chen, H. M.; Zhang, H.; Liu, B. Hierarchical Ni-Mo-S Nanosheets on Carbon Fiber Cloth: A Flexible Electrode for Efficient Hydrogen Generation in Neutral Electrolyte. *Sci. Adv.* **2015**, *1*, e1500259.

(15) Cao, B.; Veith, G. M.; Neuefeind, J. C.; Adzic, R. R.; Khalifah, P. G. Mixed Close-packed Cobalt Molybdenum Nitrides as Non-Noble Metal Electrocatalysts for The Hydrogen Evolution Reaction. *J. Am. Chem. Soc.* **2013**, *135*, 19186−19192.

(16) Yan, H.; Tian, C.; Wang, L.; Wu, A.; Meng, M.; Zhao, L.; Fu, H. Phosphorus-modified Tungsten Nitride/Reduced Graphene Oxide as A High-Performance, Non-Noble-Metal Electrocatalyst for The Hydrogen Evolution Reaction. *Angew. Chem., Int. Ed.* **2015**, *54*, 6325−6329.

(17) Wang, F.; Sun, Y.; He, Y.; Liu, L.; Xu, J.; Zhao, X.; Yin, G.; Zhang, L.; Li, S.; Mao, Q.; et al. Highly Efficient and Durable MoNiNC Catalyst for Hydrogen Evolution Reaction. *Nano Energy* **2017**, *37*, 1−6.

(18) Popczun, E. J.; Read, C. G.; Roske, C. W.; Lewis, N. S.; Schaak, R. E. Highly Active Electrocatalysis of the Hydrogen Evolution Reaction by Cobalt Phosphide Nanoparticles. *Angew. Chem., Int. Ed.* **2014**, *53*, 5427−5430.

(19) Tian, J.; Liu, Q.; Asiri, A. M.; Sun, X. Self-supported Nanoporous Cobalt Phosphide Nanowire Arrays: An Efficient 3D Hydrogen-Evolving Cathode over The Wide Range of pH 0−14. *J. Am. Chem. Soc.* **2014**, *136*, 7587−7590.

(20) Lukowski, M. A.; Daniel, A. S.; Meng, F.; Forticaux, A.; Li, L.; Jin, S. Enhanced Hydrogen Evolution Catalysis from Chemically Exfoliated Metallic MoS_2 Nanosheets. *J. Am. Chem. Soc.* **2013**, *135*, 10274−10277.

(21) Geng, X.; Sun, W.; Wu, W.; Chen, B.; Al-Hilo, A.; Benamara, M.; Zhu, H.; Watanabe, F.; Cui, J.; Chen, T. Pure and Stable Metallic Phase Molybdenum Disulfide Nanosheets for Hydrogen Evolution Reaction. *Nat. Commun.* **2016**, *7*, 10672.

(22) Chen, J. G. Carbide and Nitride Overlayers on Early Transition Metal Surfaces: Preparation, Characterization, and Reactivities. *Chem. Rev.* **1996**, *96*, 1477−1498.

(23) Zeng, M.; Li, Y. Recent Advances in Heterogeneous Electrocatalysts for the Hydrogen Evolution Reaction. *J. Mater. Chem. A* **2015**, *3*, 14942−14962.

(24) Alexander, A. M.; Hargreaves, J. S. J. *Chem. Soc. Rev.* **2010**, *39*, 4388−4401.

(25) Xiao, P.; Ge, X.; Wang, H.; Liu, Z.; Fisher, A.; Wang, X. Novel Molybdenum Carbide-Tungsten Carbide Composite Nanowires and Their Electrochemical Activation for Efficient and Stable Hydrogen Evolution. *Adv. Funct. Mater.* **2015**, *25*, 1520−1526.

(26) Xiao, P.; Yan, Y.; Ge, X.; Liu, Z.; Wang, J.-Y.; Wang, X. Investigation of Molybdenum Carbide Nano-Rod as An Efficient and Durable Electrocatalyst for Hydrogen Evolution in Acidic and Alkaline Media. *Appl. Catal., B* **2014**, *154*−*155*, 232−237.

(27) Al-Megren, H. A.; Xiao, T. C.; Gonzalez-Cortes, S. L.; Al-Khowaiter, S. H.; Green, M. L. H. Alternative Catalytic Materials: Carbides, Nitrides, Phosphides and Amorphous Boron Alloys. *J. Mol. Catal. A: Chem.* **2005**, *225*, 143−148.

(28) Enyashin, A. N.; Bar-Sadan, M. B.; Houben, L.; Seifert, G. Line Defects in Molybdenum Disulfide Layers. *J. Phys. Chem. C* **2013**, *117*, 10842−10848.

(29) Krüger, P. Molybdenum Clusters on a TiO_2 (110) Substrate Studied by Density Functional Theory. *J. Phys. Chem. C* **2009**, *113*, 5308−5312.

(30) Chen, W.-F.; Muckerman, J. T.; Fujita, E. Recent Developments in Transition Metal Carbides and Nitrides as Hydrogen Evolution Electrocatalysts. *Chem. Commun.* **2013**, *49*, 8896−8909.

(31) Wang, S.; Wang, J.; Zhu, M.; Bao, X.; Xiao, B.; Su, D.; Li, H.; Wang, Y. Molybdenum-carbide-modified Nitrogen-Doped Carbon Vesicle Encapsulating Nickel Nanoparticles: A Highly Efficient, Low-Cost Catalyst for Hydrogen Evolution Reaction. *J. Am. Chem. Soc.* **2015**, *137*, 15753−15759.

(32) Ma, R.; Zhou, Y.; Chen, Y.; Li, P.; Liu, Q.; Wang, J. Ultrafine Molybdenum Carbide Nanoparticles Composited with Carbon as A Highly Active Hydrogen-Evolution Electrocatalyst. *Angew. Chem., Int. Ed.* **2015**, *54*, 14723−14727.

(33) You, B.; Jiang, N.; Sheng, M.; Bhushan, M. W.; Sun, Y. Hierarchically Porous Urchin-Like Ni_2P Superstructures Supported on

DOI: 10.1021/acsenergylett.7b00990
ACS Energy Lett. 2018, 3, 78−84

Nickel Foam as Efficient Bifunctional Electrocatalysts for Overall Water Splitting. *ACS Catal.* **2016**, *6*, 714−721.
(34) Huang, Z.; Chen, Z.; Chen, Z.; Lv, C.; Meng, H.; Zhang, C. $Ni_{12}P_5$ Nanoparticles as An Efficient Catalyst for Hydrogen Generation via Electrolysis and Photoelectrolysis. *ACS Nano* **2014**, *8*, 8121−8129.
(35) Lee, C.-P.; Chen, W.-F.; Billo, T.; Lin, Y.-G.; Fu, F.-Y.; Samireddi, S. N.; Lee, C.-H.; Hwang, J.-S.; Chen, K.-H.; Chen, L.-C. Beaded Stream-Like $CoSe_2$ Nanoneedle Array for Efficient Hydrogen Evolution Electrocatalysis. *J. Mater. Chem. A* **2016**, *4*, 4553−4561.
(36) Liu, R.; Zhang, G.; Cao, H.; Zhang, S.; Xie, Y.; Haider, A.; Kortz, U.; Chen, B.; Dalal, N. S.; Zhao, Y.; et al. Enhanced Proton and Electron Reservoir Abilities of Polyoxometalate Grafted on Graphene for High-Performance Hydrogen Evolution. *Energy Environ. Sci.* **2016**, *9*, 1012−1023.
(37) Zhang, K.; Zhao, Y.; Zhang, S.; Yu, H.; Chen, Y.; Gao, P.; Zhu, C. MoS_2 Nanosheet/Mo_2C-Embedded N-Doped Carbon Nanotubes: Synthesis and Electrocatalytic Hydrogen Evolution Performance. *J. Mater. Chem. A* **2014**, *2*, 18715−18719.
(38) Zhang, K.; Zhao, Y.; Fu, D.; Chen, Y. Molybdenum Carbide Nanocrystals Embedded N-Doped Carbon Nanotubes as Electrocatalysts for Hydrogen Generation. *J. Mater. Chem. A* **2015**, *3*, 5783−5788.
(39) Shi, Z.; Nie, K.; Shao, Z.-J.; Gao, B.; Lin, H.; Zhang, H.; Liu, B.; Wang, Y.; Zhang, Y.; Sun, X.; et al. Phosphorus-Mo_2C@Carbon Nanowires Toward Efficient Electrochemical Hydrogen Evolution: Composition, Structural and Electronic Regulation. *Energy Environ. Sci.* **2017**, *10*, 1262−1271.
(40) Wan, C.; Regmi, Y. N.; Leonard, B. M. Multiple Phases of Molybdenum Carbide as Electrocatalysts for the Hydrogen Evolution Reaction. *Angew. Chem., Int. Ed.* **2014**, *53*, 6407−6410.
(41) Liu, Y.; Yu, G.; Li, G.-D.; Sun, Y.; Asefa, T.; Chen, W.; Zou, X. Coupling Mo_2C with Nitrogen-Rich Nanocarbon Leads to Efficient Hydrogen-Evolution Electrocatalytic Sites. *Angew. Chem., Int. Ed.* **2015**, *54*, 10752−10757.
(42) Zheng, Y.; Jiao, Y.; Jaroniec, M.; Qiao, S. Z. Advancing the Electrochemistry of the Hydrogen Evolution Reaction through Combining Experiment and Theory. *Angew. Chem., Int. Ed.* **2015**, *54*, 52−65.
(43) Xu, X.; Song, F.; Hu, X. A Nickel Iron Diselenide-Derived Efficient Oxygen-Evolution Catalyst. *Nat. Commun.* **2016**, *7*, 12324.

DOI: 10.1021/acsenergylett.7b00990
ACS Energy Lett. 2018, 3, 78−84